Chemical Engineering Journal 274 (2015) 224–230

Contents lists available at ScienceDirect

Chemical Engineering Journal

journal homepage: www.elsevier.com/locate/cej

X-shaped hollow α-FeOOH penetration twins and their conversion to α-Fe_2O_3 nanocrystals bound by high-index facets with enhanced photocatalytic activity

Hanfeng Liang [a], Wei Chen [a], Rongrong Wang [a], Zhengbing Qi [a], Jinxiao Mi [b], Zhoucheng Wang [a,*]

[a] College of Chemistry and Chemical Engineering, Xiamen University, Xiamen 361005, China
[b] College of Materials, Xiamen University, Xiamen 361005, China

HIGHLIGHTS

- X-shaped hollow α-FeOOH penetration twins were synthesized for the first time.
- X-shaped hollow α-Fe_2O_3 was formed *via* topotactic conversion of α-FeOOH precursor.
- The as-converted α-Fe_2O_3 nanostructures are bound by high-index {1 1 $\bar{2}$ 3} facets.
- X-shaped hollow α-Fe_2O_3 nanostructures show superior photocatalytic activity.

GRAPHICAL ABSTRACT

We report the facile synthesis of X-shaped α-FeOOH penetration twins and their conversion to α-Fe_2O_3 nanocrystals bound by high-index facets for highly efficient photodegradation of RhB under visible-light irradiation.

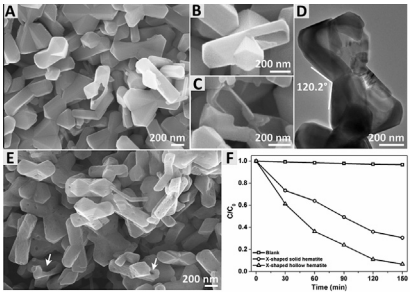

ARTICLE INFO

Article history:
Received 24 October 2014
Received in revised form 19 March 2015
Accepted 25 March 2015
Available online 7 April 2015

Keywords:
α-FeOOH
Hollow structures
Penetration twins
α-Fe_2O_3
High-index facets
Photocatalytic activity

ABSTRACT

Nonspherical hollow nanoparticles (NHNPs) have attracted a great deal of attention in recent years due to their unique properties and many promising applications. However, compared to hollow spheres, the fabrication of NHNPs is generally much more difficult and there are only a few successful examples to date. In this work, X-shaped hollow α-FeOOH penetration twins were first synthesized by a facile hydrothermal reaction. X-shaped α-Fe_2O_3 hollow nanostructures with high-index {1 1 $\bar{2}$ 3} facets exposed were further obtained *via* the topotactic transformation of α-FeOOH precursor. To the best of our knowledge, this is the first report on the nanostructures with high-index facets as well as a hollow interior. Owing to the special hollow structure and the high-energy surface, the as-obtained α-Fe_2O_3 nanocrystals show excellent visible-light photocatalytic activity toward the degradation of RhB.

1. Introduction

Owing to their promising applications in catalysis, drug delivery, gas sensor and energy storage, nonspherical hollow nanoparticles (NHNPs) have attracted fast growing interests in recent years [1–15]. Compared with the common hollow spheres, NHNPs present not only characteristic merits of hollow structure such as large surface area, well-defined voids, high permeability and low density, but also anisotropic texture correlated with multiple axes. Interestingly, NHNPs often exhibit better performances than hollow spheres although they present the same feature of a hollow interior.

* Corresponding author. Tel./fax: +86 592 2180738.
E-mail address: zcwang@xmu.edu.cn (Z. Wang).

http://dx.doi.org/10.1016/j.cej.2015.03.125
1385-8947/

For instance, Qian et al. demonstrated that Mn_2O_3 NHNPs showed better adsorption performance for phenol in comparison to its spherical hollow structures [2]. Therefore, substantial efforts have been devoted to the fabrication of NHNPs. However, different from hollow spheres, the synthesis of NHNPs is still in an embryonic stage and generally much more difficult. Although template-assisted routes are highly successful in the synthesis of hollow spheres, they bring some major limitations forward when it comes to the preparation of NHNPs: (i) the paucity of proper and easily produced nonspherical templates; (ii) the difficulty in forming uniform coatings around high-curvature surfaces and subsequent preservation of the shape with high residual stresses [4,5]. In this regard, some novel methods based on the Kirkendall effect, chemical etching and galvanic replacement have been developed for efficient production of various NHNPs [1–3,7–12]. For example, Li et al. demonstrated the synthesis of MnO_2 nanoboxes by combining the Kirkendall effect with a sacrificial crystalline template [10]. Lu et al. reported the synthesis of Pt/Ag hollow cubic nanostructures *via* a tailored galvanic replacement reaction [12]. Despite these successes, the synthesis of NHNPs still remains a great challenge. Moreover, as a major limitation, almost obtained NHNPs in previous literature are with elliptical (cocoon- or spindle-like), cubic (box-like), or octahedral (cage-like) shapes, while NHNPs with other shapes have rarely been reported.

The most fascinating part of NHNPs with shapes other than cubic or octahedral may be the fact that it makes the surfaces of NHNPs possible to be bound by high-index facets. As we know, nanocrystals with high-index facets often exhibit high activities in many processes due to their high density of atomic steps, ledges, kinks and dangling bonds on the surface [16]. Therefore, the synthesis of high-index facets is of great interest. Unfortunately, the surfaces with high energy normally disappear during the crystal growth process in order to minimize the total surface energy [17]. This makes it considerably difficult to synthesize nanocrystals bound by high-index facets. To date, only a few successful examples for metal oxides have been reported [18–22]. For example, Wang and co-workers demonstrated the preparation of Cu_2O microcrystals enclosed by {3 1 1} high-index planes [19]. Xie et al. reported the synthesis of SnO_2 octahedra with exposed high-energy {2 2 1} facets [20]. Notwithstanding these advances, the exploration of nanocrystals bound by high-index facets, especially those with complex shapes (e.g. hierarchical, porous or hollow structures) is still limited.

In this work, X-shaped hollow α-FeOOH nanostructures were first synthesized by a facile hydrothermal method. The X-shaped hollow α-FeOOH nanostructures were formed as the result of a twinning mechanism leading to so-called penetration twins. By thermal treatment of the α-FeOOH precursor, anisotropic X-shaped hollow α-Fe_2O_3 nanocrystals with exposed high-index $\{1\,1\,\bar{2}\,3\}$ facets were readily obtained. Although nanocrystals with high-index facets as well as a nonspherical hollow interior has never been reported, it can be expected that this kind of material would exhibit unexpected properties since it holds the advantages of both hollow structure and high-energy surface. Our experimental result shows that the as-obtained X-shaped hollow α-Fe_2O_3 nanocrystals exhibited high photocatalytic activity toward the degradation of Rhodamine B (RhB).

2. Experimental

2.1. Sample preparation

2.1.1. Synthesis of X-shaped hollow α-FeOOH nanostructures

X-shaped hollow α-FeOOH nanostructures were synthesized by a modified hydrothermal method [23]. In a typical synthesis route, 1 mmol of $FeCl_3{\cdot}6H_2O$, 0.2 mmol of Na_2CO_3 and 1.5 mmol of NaF were dissolved in 60 mL of deionized water. The mixture was then stirred for 20 min followed by transferring into a Teflon-lined stainless steel autoclave of 100 mL capacity. The autoclave was sealed and maintained at 200 °C for 24 h. After the autoclave was cooled to room temperature naturally, the obtained product was collected and washed several times with deionized water and ethanol, and finally dried at 60 °C for 12 h.

2.1.2. Synthesis of rod-like hollow α-FeOOH nanostructures

The procedure was the same as that for the synthesis of X-shaped hollow α-FeOOH nanostructures mentioned above except for 1 mmol of Na_2CO_3 was used and the reaction time was decreased to 12 h.

2.1.3. Synthesis of X-shaped α-FeOOH nanostructures with a solid interior

The procedure was the same as that for the synthesis of rod-like hollow α-FeOOH nanostructures mentioned above except for the reaction temperature was decreased to 150 °C.

2.1.4. Synthesis of X-shaped porous hollow α-Fe_2O_3 nanostructures

To get X-shaped porous hollow α-Fe_2O_3 nanostructures, the as-obtained X-shaped hollow α-FeOOH precursor was calcined at 500 °C for 3 h.

2.1.5. Synthesis of rod-like hollow α-Fe_2O_3 nanostructures

To get rod-like hollow α-Fe_2O_3 nanostructures, the as-obtained rod-like hollow α-FeOOH precursor was calcined at 500 °C for 3 h.

2.1.6. Synthesis of X-shaped porous α-Fe_2O_3 nanostructures with a solid interior

To get X-shaped porous α-Fe_2O_3 nanostructures, the as-obtained X-shaped α-FeOOH precursor was calcined at 500 °C for 3 h.

2.2. Sample characterization

The phase and morphology of the products were characterized by X-ray diffraction (XRD, Philips, X'pert PRO) with Cu Kα radiation (λ = 1.54056 Å), scanning electron microscopy (SEM, LEO 1530), and high-resolution transmission electron microscopy (HRTEM, JEOL JEM-2100).

2.3. Photocatalytic activity measurements

The photocatalytic activity of the catalyst was evaluated by visible light photo-degradation of Rhodamine B (RhB). In a typical test, 100 mg of X-shaped α-Fe_2O_3 hollow nanoparticles were added to 100 mL of 20 mg L^{-1} RhB solution followed by the addition of 1 mL 30 wt.% H_2O_2. The suspension was stirred in dark for 40 min to reach absorption equilibrium and then irradiated using a photochemical reactor (visible-light 420 nm, NBET HSX-F300, Beijing) under continuous stirring. Analytical samples were taken from the reaction suspension after various reaction times and centrifuged to remove the particles for analysis. UV–vis adsorption spectra were recorded at different intervals to monitor the degradation process using a Shimadzu 2550 spectrophotometer.

3. Results and discussion

In a typical synthesis of X-shaped hollow α-FeOOH nanocrystals, a mixture of $FeCl_3{\cdot}6H_2O$, Na_2CO_3 and NaF was kept at 200 °C under hydrothermal conditions for 24 h. The hollow structures

were achieved by the employment of F^- anions, which have been shown to act as an etching agent for iron oxide [3,6]. For example, Song et al. reported the fabrication of hollow hematite polyhedra by the F-assisted etching [3]. We previously demonstrated the synthesis of 2D α-Fe_2O_3 hollow microstructures by a similar F-assisted etching method [6]. Therefore, when a suitable amount of NaF was introduced into the system, it could be expected that hollow α-FeOOH nanostructures would be formed due to the specific etching. We also used a relatively high temperature (i.e. 200 °C) and a long reaction time (i.e. 24 h) to promote the etching process. As expected, the hollow version of X-shaped α-FeOOH nanocrystals was obtained. XRD was first employed to confirm the phase of the product. As shown in Fig. 1A, all the diffraction peaks are in good agreement with those of goethite (JCPDS no. 29-0713), which suggests that the as-obtained product is pure α-FeOOH. The sharp peaks also indicate the good crystalline of the α-FeOOH hollow nanoparticles.

The morphology of the product was then investigated by scanning electron microscopy (SEM) and transmission electron microscopy (TEM). A panoramic SEM image (Fig. 1B) shows that the product consists of uniform X-shaped nanostructures with smooth surfaces. The hollow interiors of the product can be directly confirmed by the SEM and TEM images of some cracked particles (Fig. 1C–E). It can be also seen clearly that the X-shaped structures are formed by two rhombic prisms crossing each other. This seemingly unusual behavior of α-FeOOH resembles the features of penetration twins observed in various natural minerals (e.g. staurolite [24]) and some synthetic materials (e.g. Fe_2P [25], Zn_2GeO_4 [26], $CaSO_4{\cdot}2H_2O$ [27] and β-FeOOH [28]). In fact, V- and Y-shaped α-FeOOH penetration twins have also been reported in previous literature [29]. Generally, the arm orientation is controlled by the crystallographic twinning [25]. In our case, the crosses are only observed with arms at ~120° angles (Fig. 1E), which supports the contention. This value is also very close to those observed in V- (118 ± 4°) and Y-shaped (119 ± 4°) α-FeOOH [29]. It is noted that penetration twins could be attributed to the twinning of two individual particles (rod-like crystals in this work), which needs to be explored in more detail in order to better understand the special X-shaped nanostructures. Very interestingly, when the synthetic parameters were slightly changed (see details in

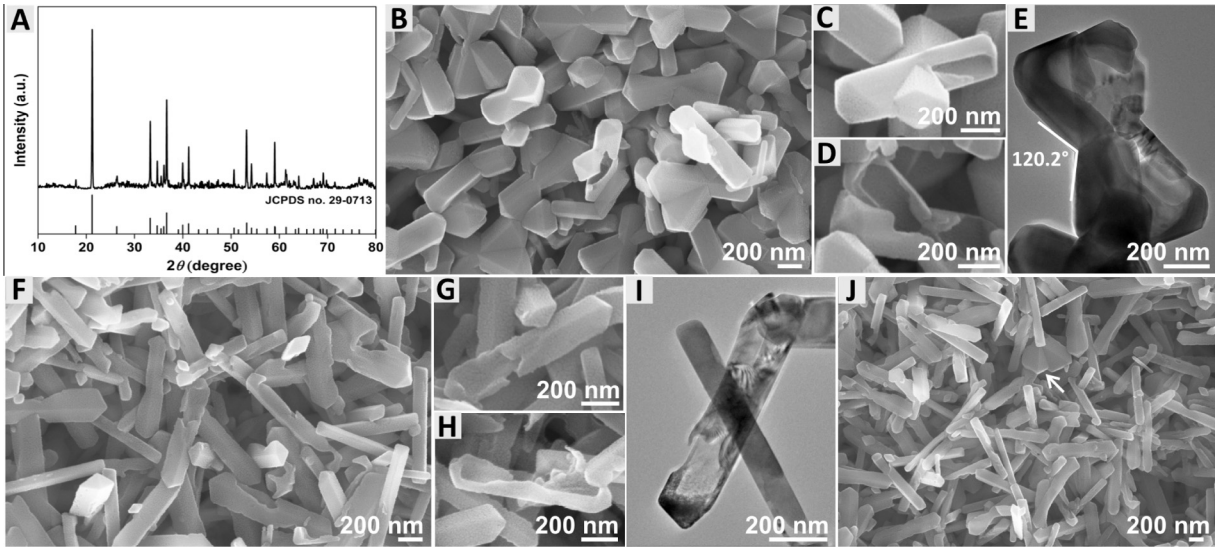

Fig. 1. (A) XRD pattern, (B)–(D) SEM and (E) TEM images of X-shaped hollow α-FeOOH penetration twins. (F)–(H) SEM and (I) TEM images of rod-like hollow α-FeOOH nanostructures. (J) shows an additional SEM image of the rod-like hollow α-FeOOH nanoparticles, from which a similar X-shaped particle (indicated by a white arrow) as that shown in (B) is observed, suggesting the X-shaped structures are formed by two rod-like particles crossing each other with certain angels.

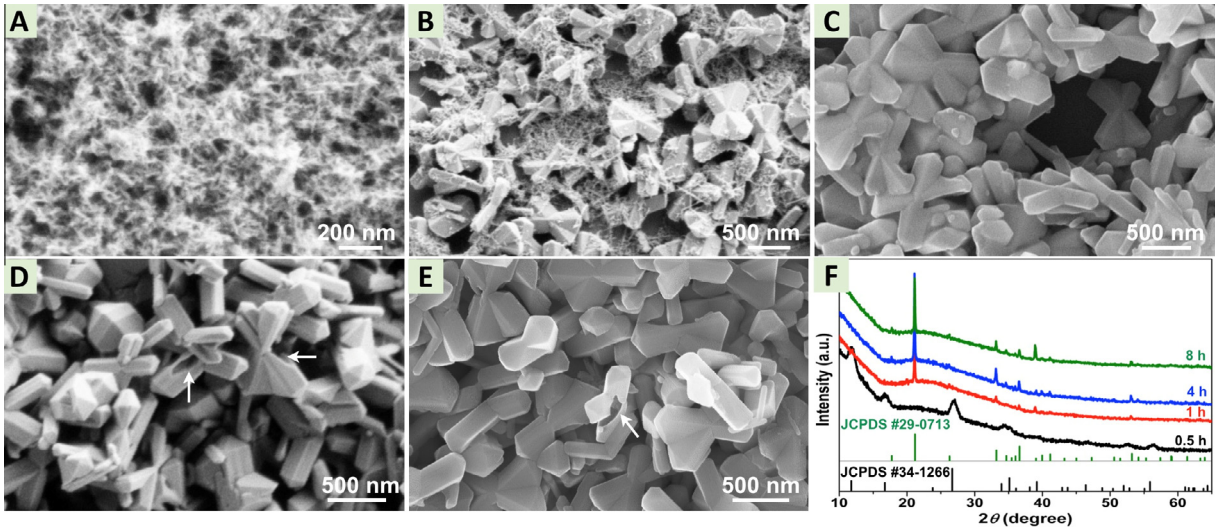

Fig. 2. SEM images (A)–(E) and XRD patterns (F) of the products obtained at different reaction times: (A) 0.5 h; (B) 1 h, (C) 4 h; (D) 8 h, and (E) 24 h.

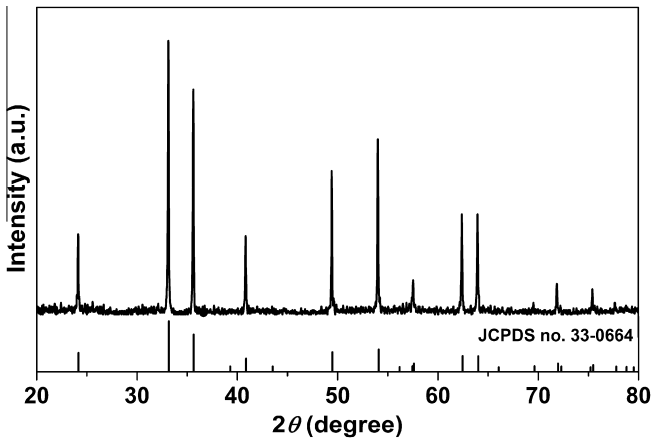

Fig. 3. XRD pattern of the X-shaped porous hollow α-Fe_2O_3 obtained by annealing α-FeOOH precursor at 500 °C for 3 h in air.

Section 2), rod-like hollow α-FeOOH nanoparticles could be readily obtained. As shown in Fig. 1F–I, the shape of the product is the same as that of the branches of X-shaped hollow α-FeOOH nanocrystals. The existence of some cracked nanoboxes shows the evidence that the product is with a hollow interior. Moreover, some X-shaped structures can be also observed although the percentage is very low, supporting the X-shaped α-FeOOH twins are formed by two rod-like α-FeOOH nanocrystals crossing each other with certain angels (Fig. 1J).

To further reveal the morphology evolution of the as-obtained X-shaped nanostructure, time-dependent experiments were performed. Fig. 2 shows the SEM images and XRD patterns of the products obtained at different reaction times. At the initial stage (e.g. 0.5 h, Fig. 2A), the product is composed of nanowires, whose phase can be clearly identified as β-FeOOH with poor crystallinity from their XRD pattern (Fig. 2F). As the reaction was prolonged to 1 h (Fig. 2B), many X-shaped nanostructures were newly formed, while nanowires were also observed. Note that the product obtained at this stage is clearly the α-FeOOH (Fig. 2F), which means there is a phase change from β-FeOOH nanowires to α-FeOOH nanowires during this period. The evolution from α-FeOOH nanowires to X-shaped α-FeOOH penetration twins is quite complicated. The formation of such penetration twins could probably go through a dissolution–recrystallization process of the previously formed α-FeOOH nanowires and subsequent an interruption in the crystal lattice during crystal growth [25]. After the reaction time was further increased to 4 h (Fig. 2C), the nanowires were completed converted to X-shaped nanostructures. As the reaction continued (e.g. 8 h, Fig. 2D), some holes were found on the surface of the X-shaped nanostructures, and finally the interior of the structure was hollowed out (Fig. 2E), leading to the formation of X-shaped hollow α-FeOOH penetration twins.

The formation of X-shaped hollow structure could be due to the dissolution of α-FeOOH caused by the F^- anions. The chemical reactions involved can be expressed as follows:

$$Fe^{3+} + 3H_2O \rightarrow Fe(OH)_3 + 3H^+ \quad (1)$$

$$Fe(OH)_3 \rightarrow \beta\text{-FeOOH} + H_2O \rightarrow \alpha\text{-FeOOH} + H_2O \quad (2)$$

$$FeOOH + 6F^- + 3H^+ \rightarrow [FeF_6]^{3-} + 2H_2O \quad (3)$$

As shown above, the hydrolysis of Fe^{3+} salt (Eq. (1)) resulted in the formation of β-FeOOH, which subsequently converted to X-shaped α-FeOOH nanostructures as discussed earlier. At initial stages, the F^- anions might absorb on the surface of the particles. While as the reaction proceeded, the F^- anions absorbed on the surface of the nanostructures accumulated, thus the F-assisted etching of α-FeOOH would be dominant (Eq. (3)), which leads to the evacuation of some holes on the surface. The surrounding H^+ ions (Eq. (1)) and the high surface energy of the structures would promote the dissolution of the α-FeOOH. It is noted that the core seems to be easier to be etched than the shell, which may be due to the poorer crystallinity of the core. As a result, X-shaped hollow α-FeOOH nanostructures were formed. Such F-assisted etching process has also been demonstrated for the preparation of hollow α-Fe_2O_3 polyhedra and hollow microstructures [3,6].

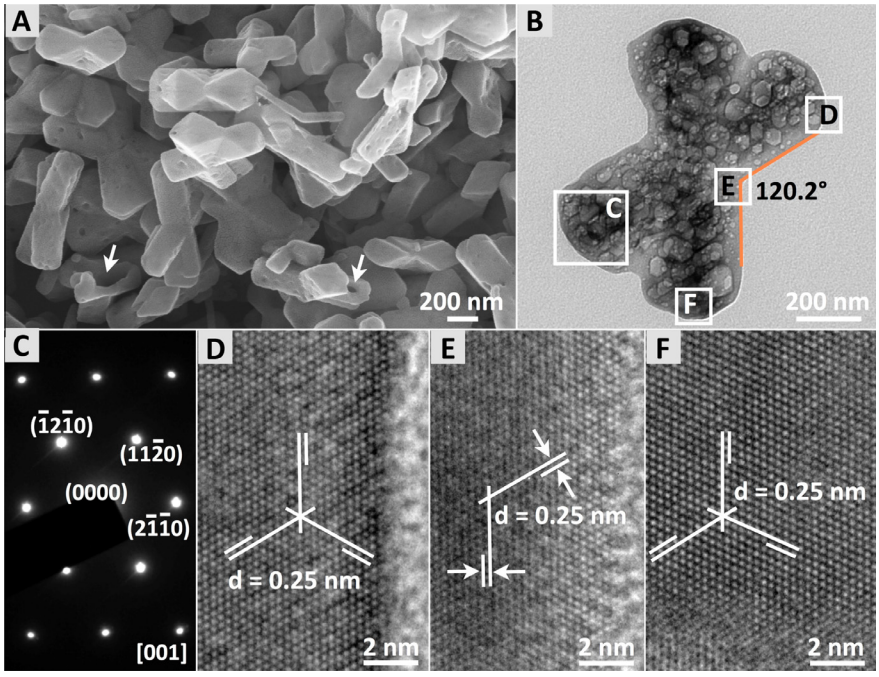

Fig. 4. (A) SEM and (B) TEM images, (C) SAED pattern and (D)–(F) HRTEM images of X-shaped porous hollow α-Fe_2O_3 obtained by annealing α-FeOOH precursor at 500 °C for 3 h in air.

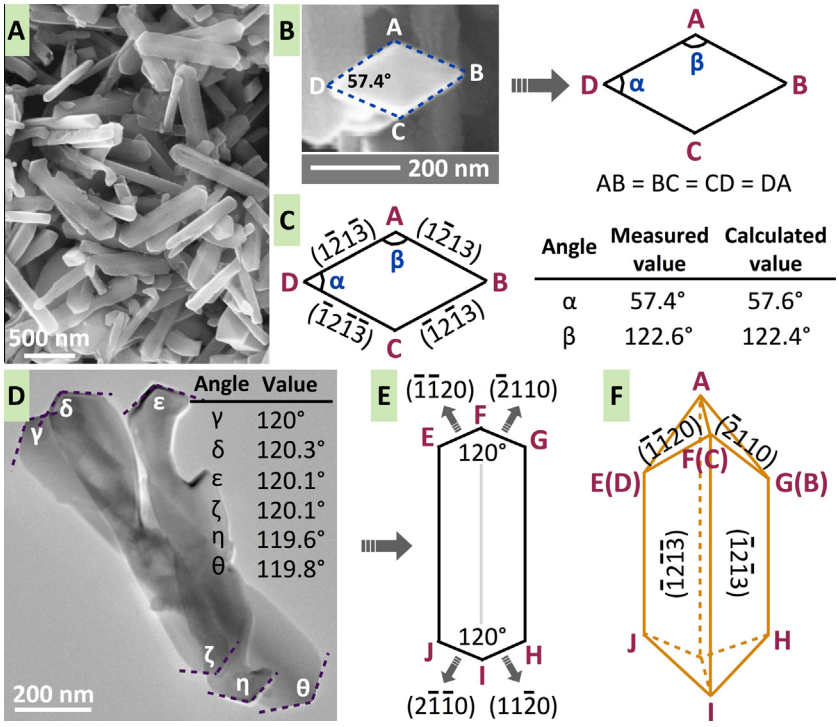

Fig. 5. Structural characterization of rod-like α-Fe_2O_3 nanocrystals. (A) SEM image. (B) SEM image and corresponding 2D model of the top branch of an individual particle. The shape observed from Fig. 3B is perfectly matched with a rhombus (AB = BC = CD = DA), indicating the viewing angle is 90°. Therefore, the measured values of dihedral angles should be very close to the actual values. (C) Comparison of the measured and calculated values of dihedral angles. (D) and (E) TEM image and corresponding 2D model of the rod-like α-Fe_2O_3 nanocrystals. (F) An ideal 3D geometrical model of rod-like α-Fe_2O_3 nanocrystals with 4 {1 1 $\bar{2}$ 0} and 4 high-index {1 1 $\bar{2}$ 3} facets.

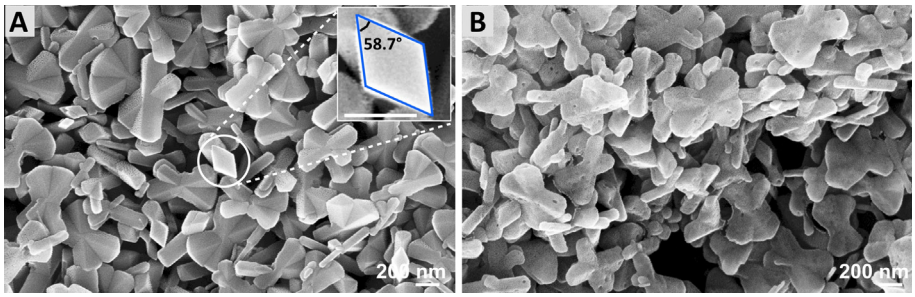

Fig. 6. SEM images of (A) X-shaped α-FeOOH nanostructures with a solid interior and (B) X-shaped α-Fe_2O_3 nanostructures with a solid interior obtained by annealing α-FeOOH precursor at 500 °C for 3 h.

As the most stable iron oxide under ambient conditions, α-Fe_2O_3 has been extensively investigated and widely used in many fields. Various α-Fe_2O_3 nanostructures have been prepared as they were expected to show unique shape-dependent properties [6,14,30–33]. Among them, NHNPs is of particular interest. Much effort has been dedicated to preparing α-Fe_2O_3 NHNPs with the aim of exploring their shape-dependent properties. For example, we recently demonstrated the synthesis of hollow α-Fe_2O_3 nanospindles by a facile hydrothermal method [14]. Nonetheless, the fabrication of α-Fe_2O_3 NHNPs is still limited. Herein, X-shaped hollow α-Fe_2O_3 nanocrystals can be readily obtained by dehydration of α-FeOOH precursor *via* a topotactic transformation [34]. The XRD analysis confirms the formation of hematite phase (JCPDS no. 33-0664) with high crystallinity and purity (Fig. 3).

Fig. 4 shows the SEM and TEM images of α-Fe_2O_3 nanostructures obtained by annealing α-FeOOH precursor at 500 °C for 3 h in air. The overall morphology appears unchanged compared with that of X-shaped α-FeOOH precursor. Due to the volume contraction associated with the transformation from low density (4.3 g cm^{-3}) α-FeOOH to denser hematite (5.3 g cm^{-3}), many pores are introduced during the annealing process. Meanwhile, some broken holes (as indicated by white arrows in Fig. 4A) can be seen clearly, revealing the α-Fe_2O_3 nanostructures obtained after annealing are still with a hollow interior. It is noted that the angles between two branches are measured to be ~120° (Fig. 4B), which is perfectly matched with the value measured for X-shaped α-FeOOH structures (Fig. 1E). To gain insights into the morphological detail, the X-shaped α-Fe_2O_3 nanostructures were further investigated by TEM. Fig. 4C shows the selected area electron diffraction (SAED) pattern of one branch (indicated by a square in Fig. 4B) of the X-shaped α-Fe_2O_3 nanostructures, revealing the single-crystal nature of the branch. Fig. 4D–F shows the high-resolution TEM (HRTEM) images of areas marked by squares in Fig. 4B. The lattice spacings are measured to be 0.25 nm, which is in agreement with the {1 1 $\bar{2}$ 0} lattice spacing of rhombohedral hematite. The special X-shaped structure makes it difficult to identify the Miller indices of the nanocrystals. To simplify this issue, we also synthesized α-Fe_2O_3 nanorods by annealing rod-like α-FeOOH precursor at 500 °C for 3 h.

As shown in Fig. 5A, the product composes of rhombic prisms with two pointed ends, which are the same as the shape observed in rod-like α-FeOOH precursor. The dihedral angle between two

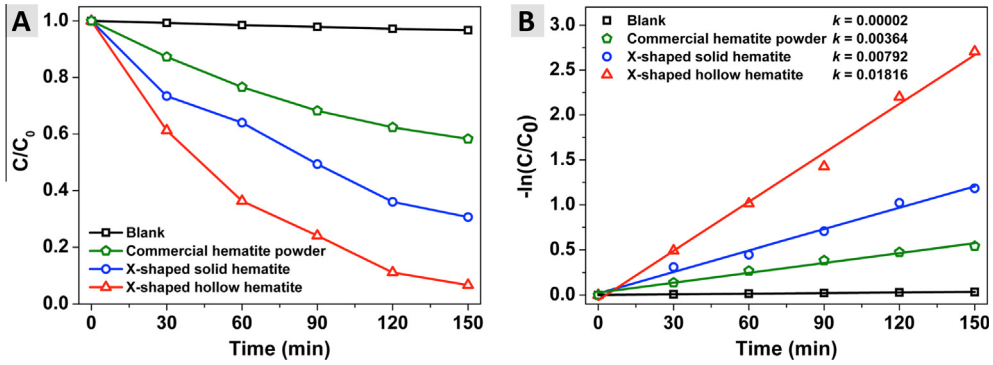

Fig. 7. (A) Photodegradation of RhB over commercial α-Fe_2O_3 powder and the as-obtained X-shaped hollow and solid α-Fe_2O_3 nanocrystals. *C* is the concentration of RhB at the irradiation time *t* and C_0 is the initial concentration of RhB. (B) Comparison of the apparent reaction rate constants (*k*) based on the pseudo-first-order reaction kinetics.

Table 1
Comparison of the photocatalytic activity of the X-shaped hollow α-Fe_2O_3 nanostructures and other reported hollow structure toward the degradation of RhB under visible-light irradiation.

Catalyst/amount	Conditions	Degradation of RhB	Reference
X-shaped hollow α-Fe_2O_3 nanostructures/100 mg	100 mL of 20 mg/L RhB (~4×10^{-5} M) + 1 mL 30 wt.% H_2O_2	94% in 150 min	This work
α-Fe_2O_3 cage-like hollow spheres/50 mg	20 mL RhB (1×10^{-5} M) + 0.1 mL 30 wt.% H_2O_2	~60% in 180 min	[35]
Single-shelled α-Fe_2O_3 hollow spheres/200 mg	100 mL of 5 mg/L RhB (~1×10^{-5} M) + 0.5 mL 30 wt.% H_2O_2	~40% in 120 min	[36]
Multi-shelled α-Fe_2O_3 hollow spheres/200 mg	100 mL of 5 mg/L RhB (~1×10^{-5} M) + 0.5 mL 30 wt.% H_2O_2	~92% in 120 min	[36]
α-Fe_2O_3 hollow microstructures/100 mg	100 mL of 20 mg/L RhB (~4×10^{-5} M) + 1 mL 30 wt.% H_2O_2	~70% in 180 min	[6]
α-Fe_2O_3 hollow polyhedra/50 mg	60 mL of 20 mg/L RhB (~4×10^{-5} M) + 1 mL 30 wt.% H_2O_2	~94% in 150 min	[37]
γ-Fe_2O_3/TiO_2 Janus hollow bowls/50 mg	20 mL RhB (1×10^{-5} M)	~70% in 180 min	[38]
α-Fe_2O_3/TiO_2 core shell structures/5 mg	50 mL RhB (2×10^{-5} M)	~65% in 100 min	[39]

adjacent facets is measured to be ~57.4° (Fig. 5B). For hematite, the relationship between dihedral angles of two crystal facets and their Miller indices can be expressed as follows:

$$\cos\varphi = \frac{h_1h_2 + k_1k_2 + \frac{1}{2}(h_1k_1 + h_2k_2)\frac{3a^2}{4c^2}l_1l_2}{\sqrt{\left(h_1^2 + k_1^2 + h_1k_1 + \frac{3a^2}{4c^2}l_1^2\right)\left(h_2^2 + k_2^2 + h_2k_2 + \frac{3a^2}{4c^2}l_2^2\right)}} \quad (4)$$

where φ is the dihedral angle, *h*, *k*, *l* are the Miller indices, and *a*, *c* are the cell parameters (a = 5.0356 Å, c = 13.7489 Å). The above equation can be used to check if the two facets with known Miller indices are correct. By comparing the measured and calculated values of the dihedral angle, the four facets of the prisms can be indexed to {1 1 $\bar{2}$ 3} facets (Fig. 5C). Fig. 5D shows the TEM image of the rod-like α-Fe_2O_3 crystals. It can be seen that the angles of the pointed ends are ~120°. Similarly, the facets can be calculated to be {1 1 $\bar{2}$ 0} facets. Therefore, we can infer that the X-shaped hollow α-Fe_2O_3 nanocrystals are bound by {1 1 $\bar{2}$ 0} facets and high-index {1 1 $\bar{2}$ 3} facets.

The as-obtained X-shaped hollow α-Fe_2O_3 nanocrystals were then evaluated as photocatalysts for the degradation of RhB under visible-light irradiation. For comparison, X-shaped α-Fe_2O_3 nanocrystals with a solid interior have also been synthesized by annealing the corresponding α-FeOOH precursor (see synthetic details in Section 2). From the SEM image of the X-shaped α-FeOOH with a solid interior (Fig. 6), it can be seen that the shape of the end of one branch is perfectly matched with a rhombus. The value of the dihedral angle is measured to be ~58.7°, which is in good agreement with that of rod-like α-Fe_2O_3 nanostructures (Fig. 5B). This result indicates that the conversion from α-FeOOH to α-Fe_2O_3 undergoes a topotactic transformation process [34]. And it also further confirms that the X-shaped α-FeOOH twins are generated by two rod-like α-FeOOH prisms in the way of crossing each other. After thermal treatment, the X-shaped α-FeOOH completely converts to porous X-shaped α-Fe_2O_3.

Fig. 7 shows the change in RhB concentration over the photodegradation. As it can be seen, the self-degradation of RhB is negligible. While when α-Fe_2O_3 particles are added, the photodegradation rates increase significantly, and the photocatalytic activity of X-shaped α-Fe_2O_3 nanostructures is obviously much higher than that of commercial α-Fe_2O_3 powder. 70% and 94% degradation of RhB can be achieved in 150 min for X-shaped solid and hollow α-Fe_2O_3 nanocrystals, respectively (Fig. 7A). For the X-shaped hollow α-Fe_2O_3 nanocrystals, the photocatalytic activity toward the degradation of RhB under visible-light irradiation is higher than or at least comparable to other reported hollow structures (see comparison in Table 1). The high performances can be attributed to the high-energy surface. The photocatalytic degradation of RhB over α-Fe_2O_3 nanostructures has been shown to follow the pseudo-first-order reaction kinetics [40,41]. Therefore, here the pseudo-first-order model was directly used to describe the kinetic behavior of the photoreaction. The apparent reaction rate constant (*k*) of RhB degradation was also calculated to evaluate the reactivity of the catalysts quantitatively. As shown in Fig. 7B, the self-degradation rate of RhB is quite slow, with an apparent reaction

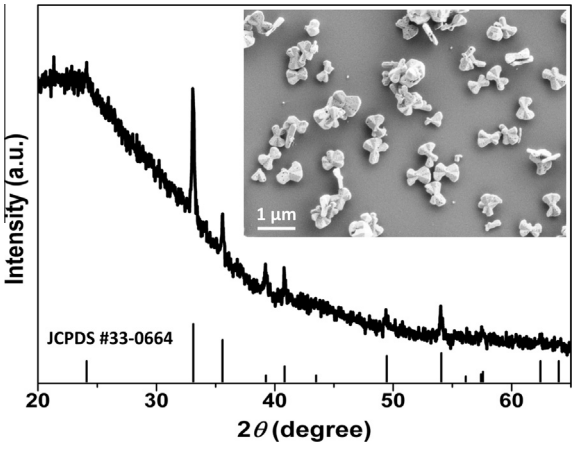

Fig. 8. XRD pattern and SEM image (inset) of the X-shaped hollow α-Fe_2O_3 nanostructures after photoreaction.

rate constant $k = 0.00002\ min^{-1}$. While for the experiments with α-Fe_2O_3 nanocrystals, the degradation rates of RhB are dramatically promoted. And the calculated values of k are 0.00364, 0.00792 and $0.01816\ min^{-1}$ for commercial α-Fe_2O_3 powder, X-shaped solid, and hollow α-Fe_2O_3 nanocrystals, respectively, suggesting the X-shaped hollow α-Fe_2O_3 nanocrystals are more active than their solid counterparts and bulk material. Apart from the high-index surfaces, their different specific surface area (16.38 and $11.77\ m^2\ g^{-1}$ for hollow and solid α-Fe_2O_3 nanocrystals, respectively) should be also responsible for the difference. The higher surface area provides more reaction sites, which are favorable for the catalytic reactions. The X-shaped hollow α-Fe_2O_3 nanocrystals also show a good stability during the test. No significant structural distortion or phase change is observed after the photocatalysis although the crystallinity seems to become poorer (Fig. 8).

4. Conclusions

In summary, X-shaped hollow α-Fe_2O_3 nanocrystals with high-index $\{1\ 1\ \bar{2}\ 3\}$ facets exposed have been synthesized for the first time. Owing to their unique hollow structure and high-energy surface, the as-obtained product showed high photocatalytic activity and stability for the photodegradation of RhB. The samples prepared in this work may also find promising applications in other fields such as sensors and energy storage.

Acknowledgments

This work was supported by the State Key Development Program for Basic Research of China (Grant No. 2007CB935603) and the National Natural Science Foundation of China (Grant No. 51372212).

References

[1] E. González, J. Arbiol, V.F. Puntes, Carving at the nanoscale: sequential galvanic exchange and Kirkendall growth at room temperature, Science 384 (2011) 1377–1380.
[2] J. Cao, Y. Zhu, K. Bao, L. Shi, S. Liu, Y. Qian, Microscale Mn_2O_3 hollow structures: sphere, cube, ellipsoid, dumbbell, and their phenol adsorption properties, J. Phys. Chem. C 113 (2009) 17755–17760.
[3] H.J. Song, X.H. Jia, X.Q. Zhang, Controllable fabrication, growth mechanism, and gas sensing properties of hollow hematite polyhedra, J. Mater. Chem. 22 (2012) 22699–22705.
[4] X.W. Lou, C. Yuan, L.A. Archer, Double-walled SnO_2 nano-cocoons with movable magnetic cores, Adv. Mater. 19 (2007) 3328–3332.
[5] J. Nai, Y. Tian, X. Guan, L. Guo, Pearson's principle inspired generalized strategy for the fabrication of metal hydroxide and oxide nanocages, J. Am. Chem. Soc. 135 (2013) 16082–16091.
[6] H. Liang, W. Chen, X. Jiang, X. Xu, B. Xu, Z. Wang, Synthesis of 2D hollow hematite microplatelets with tuneable porosity and their comparative photocatalytic activities, J. Mater. Chem. A 2 (2014) 4340–4346.
[7] K. An, S.G. Kwon, M. Park, H.B. Na, S.I. Baik, J.H. Yu, D. Kim, J.S. Son, Y.W. Kim, I.C. Song, W.K. Moon, H.M. Park, T. Hyeon, Synthesis of uniform hollow oxide nanoparticles through nanoscale acid etching, Nano Lett. 8 (2008) 4252–4258.
[8] Y. Xiong, B. Wiley, J. Chen, Z.Y. Li, Y. Yin, Y. Xia, Corrosion-based synthesis of single-crystal Pd nanoboxes and nanocages and their surface plasmon properties, Angew. Chem. Int. Ed. 44 (2005) 7913–7917.
[9] Y. Sui, W. Fu, Y. Zeng, H. Yang, Y. Zhang, H. Chen, Y. Li, M. Li, G. Zou, Synthesis of Cu_2O nanoframes and nanocages by selective oxidative etching at room temperature, Angew. Chem. Int. Ed. 49 (2010) 4282–4285.
[10] J. Fei, Y. Cui, X. Yan, W. Qi, Y. Yang, K. Wang, Q. He, J. Li, Controlled preparation of MnO_2 hierarchical hollow nanostructures and their application in water treatment, Adv. Mater. 20 (2008) 452–456.
[11] J. Lian, K. Anggara, M. Lin, Y. Chan, Formation of hollow iron oxide tetrapods via a shape-preserving nanoscale Kirkendall effect, Small 10 (2014) 667–673.
[12] W. Zhang, J. Yang, X. Lu, Tailoring galvanic replacement reaction for the preparation of Pt/Ag bimetallic hollow nanostructures with controlled number of voids, ACS Nano 6 (2012) 7397–7405.
[13] H. Liang, Z. Wang, Facile synthesis and photocatalytic activity of cocoon-like hollow hematite nanostructures, Mater. Lett. 96 (2013) 12–15.
[14] H. Liang, X. Xu, W. Chen, B. Xu, Z. Wang, Facile synthesis of hematite nanostructures with controlled hollowness and porosity and their comparative photocatalytic activities, CrystEngComm 16 (2014) 959–963.
[15] W. Yang, Y. Wang, A. Etogo, J. Ning, Y. Xie, Y. Hu, Carbon nanocoating: an effective nanoreactor towards well-defined carbon-coated GaN hollow nanospindles, Nanoscale 6 (2014) 3051–3054.
[16] Z.Y. Zhou, N. Tian, J.T. Li, I. Broadwell, S.G. Sun, Nanomaterials of high surface energy with exceptional properties in catalysis and energy storage, Chem. Soc. Rev. 40 (2011) 4167–4185.
[17] Z.Y. Jiang, Q. Kuang, Z.X. Xie, L.S. Zheng, Syntheses and properties of micro/nanostructured crystallites with high-energy surfaces, Adv. Funct. Mater. 20 (2010) 3634–3645.
[18] H. Liang, X. Jiang, Z. Qi, W. Chen, Z. Wu, B. Xu, Z. Wang, J. Mi, Q. Li, Hematite concave nanocubes and their superior catalytic activity for low temperature CO oxidation, Nanoscale 6 (2014) 7199–7203.
[19] M. Leng, M. Lu, Y. Zhang, Z. Wang, C. Yu, X. Yang, H. Zhang, C. Wang, Polyhedral 50-facet Cu_2O microcrystals partially enclosed by 311 high-index planes: synthesis and enhanced catalytic CO oxidation activity, J. Am. Chem. Soc. 132 (2010) 17084–17087.
[20] X. Han, M. Jin, S. Xie, Q. Kuang, Z. Jiang, Y. Jiang, Z. Xie, L. Zheng, Synthesis of tin dioxide octahedral nanoparticles with exposed high-energy 221 facets and enhanced gas-sensing properties, Angew. Chem. Int. Ed. 48 (2009) 9180–9183.
[21] X. Wang, C. Liu, B. Zhang, Y. Jiang, L. Zhang, Z. Xie, L. Zheng, Controlled synthesis of concave Cu_2O microcrystals enclosed by hhl high-index facets and enhanced catalytic activity, J. Mater. Chem. A 1 (2013) 282–287.
[22] H.G. Yang, C.H. Sun, S.Z. Qiao, J. Zou, G. Liu, S.C. Smith, H.M. Cheng, G.Q. Lu, Anatase TiO_2 single crystals with a large percentage of reactive facets, Nature 453 (2008) 638–641.
[23] Z.F. Dou, C.Y. Cao, Q. Wang, J. Qu, Y. Yu, W.G. Song, Synthesis, self-assembly, and high performance in gas sensing of X-shaped iron oxide crystals, ACS Appl. Mater. Interfaces 4 (2012) 5698–5703.
[24] I. Sunagawa, Crystals: Growth, Morphology, and Perfection, Cambridge University Press, Cambridge, UK, 2005.
[25] A.T. Kelly, I. Rusakova, T. Ould-Ely, C. Hofmann, A. Lüttge, K.H. Whitmire, Iron phosphide nanostructures produced from a single-source organometallic precursor: nanorods, bundles, crosses, and spherulites, Nano Lett. 7 (2007) 2920–2925.
[26] Q. Liu, Y. Zhou, Z. Tian, X. Chen, J. Gao, Z. Zou, Zn_2GeO_4 crystal splitting toward sheaf-like, hyperbranched nanostructures and photocatalytic reduction of CO_2 into CH_4 under visible light after nitridation, J. Mater. Chem. 22 (2012) 2033–2038.
[27] M. Rubbo, M. Bruno, F.R. Massaro, D. Aquilano, The five twin laws of gypsum ($CaSO_4{\cdot}2H_2O$): a theoretical comparison of the interfaces of the penetration twins, Cryst. Growth Des. 12 (2012) 3018–3024.
[28] J.H.L. Watson, R.R. Cardell, The internal structure of colloidal crystals of β-FeOOH and remarks on their assemblies in Schiller layers, J. Phys. Chem. 66 (1962) 1757–1763.
[29] H. Yang, X. Mao, Y. Guo, D. Wang, G. Ge, R. Yang, X. Qiu, Y. Yang, C. Wang, Y. Wang, G. Liu, Porous α-Fe_2O_3 nanostructures with branched topology: growth, formation mechanism, and properties, CrystEngComm 12 (2010) 1842–1849.
[30] H. Liang, B. Xu, Z. Wang, Self-assembled 3D flower-like α-Fe_2O_3 microstructures and their superior capability for heavy metal ion removal, Mater. Chem. Phys. 141 (2013) 727–734.
[31] E. Esmaeili, M. Salavati-Niasari, F. Mohandes, F. Davar, H. Seyghalkar, Modified single-phase hematite nanoparticles via a facile approach for large-scale synthesis, Chem. Eng. J. 170 (2011) 278–285.
[32] H. Liang, W. Chen, Y. Yao, Z. Wang, Y. Yang, Hydrothermal synthesis, self-assembly and electrochemical performance of α-Fe_2O_3 microspheres lithium ion batteries, Ceram. Int. 40 (2014) 10283–10290.
[33] X.L. Cheng, J.S. Jiang, C.Y. Jin, C.C. Lin, Y. Zeng, Q.H. Zhang, Cauliflower-like α-Fe_2O_3 microstructures: toluene–water interface-assisted synthesis, characterization, and applications in wastewater treatment and visible-light photocatalysis, Chem. Eng. J. 236 (2014) 139–148.
[34] Y. Cudennec, A. Lecerf, Topotactic transformations of goethite and lepidocrocite into hematite and maghemite, Solid State Sci. 7 (2005) 520–529.
[35] J. Yu, X. Yu, B. Huang, X. Zhang, Y. Dai, Hydrothermal synthesis and visible-light photocatalytic activity of novel cage-like ferric oxide hollow spheres, Cryst. Growth Des. 9 (2009) 1474–1480.
[36] Y. Liu, C. Yu, W. Dai, X. Gao, H. Qian, Y. Hu, X. Hu, One-pot solvothermal synthesis of multi-shelled α-Fe_2O_3 hollow spheres with enhanced visible-light photocatalytic activity, J. Alloys Compd. 551 (2013) 440–443.
[37] B. Xu, B. Huang, H. Cheng, Z. Wang, X. Qin, X. Zhang, Y. Dai, α-Fe_2O_3 hollow structures: formation of single crystalline thin shells, Chem. Commun. 48 (2012) 6529–6531.
[38] F. Mou, L. Xu, H. Ma, J. Guan, D. Chen, S. Wang, Facile preparation of magnetic γ-Fe_2O_3/TiO_2 Janus hollow bowls with efficient visible-light photocatalytic activities by asymmetric shrinkage, Nanoscale 4 (2012) 4650–4657.
[39] Y. Xia, L. Yin, Core-shell structured α-Fe_2O_3/TiO_2 nanocomposites with improved photocatalytic activity in the visible light region, Phys. Chem. Chem. Phys. 15 (2013) 18627–18634.
[40] Y. Zhao, F. Pan, H. Li, T. Niu, G. Xu, W. Chen, Facile synthesis of uniform α-Fe_2O_3 crystals and their facet-dependent catalytic performance in the photo-Fenton reaction, J. Mater. Chem. A 1 (2013) 7242–7246.
[41] X. Zhou, Q. Xu, W. Lei, T. Zhang, X. Qi, G. Liu, K. Deng, J. Yu, Origin of tunable photocatalytic selectivity of well-defined α-Fe_2O_3 nanocrystals, Small 10 (2014) 674–679.